GEOLOGY | THE GEOLOGICAL SOCIETY OF AMERICA®

https://doi.org/10.1130/G52138.1

Manuscript received 11 February 2024
Revised manuscript received 4 June 2024
Manuscript accepted 16 June 2024

Published online 9 July 2024

Coprecipitation of amorphous silica and gold nanoparticles contributes to gold hyperenrichment

Rory R. McNab*, Joël Brugger, Christopher R. Voisey, and Andrew G. Tomkins
School of Earth, Atmosphere & Environment, Monash University, Clayton, Victoria 3800, Australia

ABSTRACT

Hyperenrichment of Au in orogenic ores occurs overwhelmingly within quartz veins, but the formation pathway of quartz veins in orogenic systems remains enigmatic. We conducted hydrothermal experiments simulating coprecipitation of Au and amorphous silica and subsequent recrystallization to test whether this is a viable mechanism to generate Au nuggets within quartz veins. Within minutes, coprecipitation of amorphous silica and Au nanoparticles occurred, representing an effective Au deposition mechanism. Within one week, amorphous silica had recrystallized to quartz, causing the coarsening of Au particles and their relocation to quartz grain boundaries and fractures. The experimental textures are similar to those observed in high-grade zones of orogenic gold deposits. In addition to trapping Au, amorphous silica may increase competency contrasts that facilitate short-term fracture reactivation during earthquake aftershock periods or swarms, allowing further Au input from fresh fluids. These findings demonstrate that amorphous silica precipitation may be an important transient stage in orogenic gold deposit formation, with significant implications for metal accumulation in quartz veins.

INTRODUCTION

Orogenic gold deposits (OGDs) are fault-hosted hydrothermal deposits that have accounted for ≥30% of global Au production (Frimmel, 2008). One of the distinguishing features of OGDs is their extreme Au enrichment (1 to locally >100,000 ppm Au), in many cases, almost exclusively within quartz veins. The current paradigm postulates that dissolved Au precipitates together with quartz within rock fractures from dilute hydrothermal fluids in response to changes in temperature, pressure, and fluid chemistry (Cox et al., 1995). However, the maximum concentrations of dissolved Au in most orogenic-type hydrothermal fluids range between 0.010 and 1.0 ppm (Williams-Jones et al., 2009), and most crustal fluids are likely to be significantly Au-undersaturated (Rauchenstein-Martinek et al., 2014). This makes it difficult to explain the widespread formation of high-grade Au domains (>>50 ppm) in OGDs. The cyclic "fault-valve" model of Sibson et al. (1988) convincingly explains grade buildup through numerous fluid-infiltration events, based on laminated veins at macroscale and cathodoluminescence banding at microscale. However, once each layer of the vein is sealed by a new layer, gold is trapped in place, preventing gold grain growth to form coarse Au grains. Additionally, textural evidence for such cyclical fluid introduction is missing in many high-grade Au-quartz veins (Petrella et al., 2020). For these reasons, numerous processes that may contribute to Au accumulation have been investigated, including remobilization and polymetallic melt transport of Au (Hastie et al., 2021; Tooth et al., 2008). Here, we focused on the role of Au nanoparticles (AuNPs), a form of fluid-mobile Au that can be enriched up to ~5000 times more than aqueous Au (Liu et al., 2019).

Herrington and Wilkinson (1993) used textural observations from epithermal deposits and OGDs to suggest that colloidal silica and colloidal Au may in some cases be the precursors to quartz and coarse Au, respectively. In this model, formation of amorphous silica ($aSiO_2$) follows simultaneous deposition of colloidal silica and Au. Since then, the preservation of AuNPs within $aSiO_2$ domains has been observed in several OGDs (Petrella et al., 2020, 2022), and it has been demonstrated that formation of colloidal silica stabilizes AuNPs and stops their aggregation, potentially enabling long-distance transport of AuNPs (Liu et al., 2019). Yet, due to a lack of experimental evidence, the processes associated with this model remain enigmatic. In this study, we observed the transition from Au-bearing colloidal silica gel to coarse Au and quartz in experiments conducted at upper-crustal conditions.

METHOD

Circumneutral pH solutions containing colloidal silica gel (1.6 wt% SiO_2), 1–2 wt% NaCl, and 20 ppm Au were placed within Ti autoclaves and heated to 400 °C at 400 bar autogenous pressure for durations between 10 min and 1 wk (for further experimental details, see Table S1 in the Supplemental Material[1]). $AuCl_3$ was used as the dissolved Au species because it is stable under ambient conditions but reduces to AuNPs at the experimental conditions (Pokrovski et al., 2014). Following quenching, the fluid fractions were analyzed by inductively coupled plasma–optical emission spectroscopy (ICP-OES) for their Au concentrations, and the solids were analyzed by X-ray diffraction (XRD) for phase identification and by scanning electron microscopy (SEM) via secondary electron (SE) and backscatter electron (BSE) imaging for textural analysis. SEM-based energy-dispersive X-ray analysis (EDX) was also used for semiquantitative elemental micro-analyses. The size distribution of Au nanoparticles was assessed on selected BSE images using ImageJ.

RESULTS

After 10 min at 400 °C (Fig. 1A), Au dispersed throughout the $aSiO_2$ precipitate in the form of nanometer-sized particles (100 nm mean diameter; Fig. 2). A few quartz crystals were present and displayed a high density of AuNPs on their boundaries and in fractures in the sur-

Rory R. McNab https://orcid.org/0009-0007-0561-4895
*rory.mcnab1@monash.edu

[1]Supplemental Material. Details of the experiment and analysis. Please visit https://doi.org/10.1130/GEOL.S.26072635 to access the supplemental material; contact editing@geosociety.org with any questions.

CITATION: McNab, R.R., et al., 2024, Coprecipitation of amorphous silica and gold nanoparticles contributes to gold hyperenrichment: Geology, v. XX, p. , https://doi.org/10.1130/G52138.1

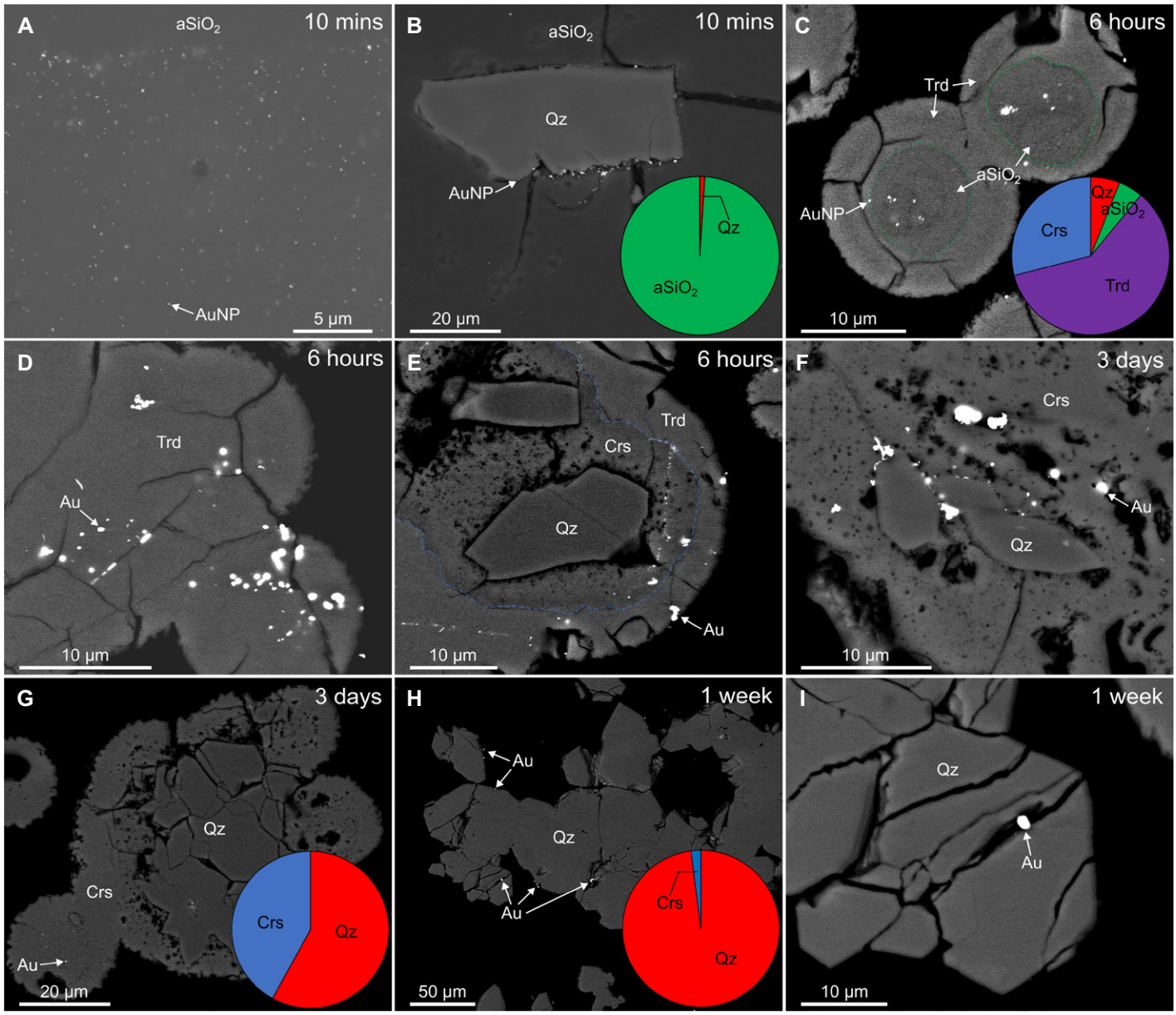

Figure 1. Experimental products after 10 min at 400 °C: (A) dispersed Au nanoparticles (AuNPs; bright spots) in an amorphous silica ($aSiO_2$) mass and (B) quartz (Qz) in $aSiO_2$ and silica ratios (wt%) pie chart of 10 min sample. Experimental products after 6 h at 400 °C: (C) microspheres, with fractured tridymite (Trd) rims and $aSiO_2$ cores with AuNPs present, and silica ratios (wt%) pie chart of 6 h sample, (D) tridymite with Au inclusions and Au-bearing fractures, and (E) porous cristobalite (Crs) recrystallization from within tridymite microspheres, and quartz recrystallization from core of cristobalite. Experimental products after 3 d at 400 °C: (F) Au in pores/fractures/grain boundaries within cristobalite (Crs) and around recrystallized quartz (Qz) grains and (G) quartz and cristobalite, and silica ratios (wt%) pie chart of 3 d sample. Experimental products after 1 wk at 400 °C: (H) silica ratios (wt%) pie chart of 1 wk sample, and quartz with Au at grain boundaries and (I) within fractures. Pie charts are based on semiquantitative X-ray diffraction data (Table S2 [see text footnote 1]).

rounding $aSiO_2$ (Fig. 1B). These AuNPs were coarser than those dispersed in $aSiO_2$ (167 vs. 100 nm mean diameter; Fig. 2). After a short time (6 h at 400 °C), most $aSiO_2$ recrystallized to tridymite ± cristobalite (Fig. 1C). Tridymite recrystallization began at the rim and progressed inward to the cores of silica microspheres (Fig. 1C). Au was coarser within the tridymite than in the original $aSiO_2$ (345 nm mean diameter; Fig. 2). AuNPs were distributed within tridymite and also along fractures and grain boundaries (Fig. 1D). Recrystallization of the tridymite to cristobalite and then to quartz occurred from the center of the microspheres, with increased porosity in the cristobalite (Fig. 1E). Au particles were absent in the recrystallized grains. However, at longer experiment time (3 d at 400 °C), aggregation and subsequent enrichment of Au occurred in the boundaries of recrystallized grains and pores in proximity to recrystallized grains (Fig. 1F; 410 nm mean diameter; Fig. 2). Over these longer durations, there was complete recrystallization of cristobalite to quartz (3 d vs. 1 wk at 400 °C; Figs. 1G and 1H). Once quartz recrystallization was complete, Au was found as sparse enlarged grains along quartz grain boundaries and fractures (1 wk at 400 °C; Figs. 1H and 1I; 976 nm mean diameter; Fig. 2).

Measurements following quenching found that Au was not detectable in the fluid after more than 10 min at 400 °C (Table S1).

DISCUSSION

Amorphous Silica in Orogenic Systems

The initial precipitation of $aSiO_2$ followed by its recrystallization, potentially via metastable silica phases, to quartz is well established for shallow, low-temperature (<300 °C) hydrothermal systems (Borhara and Onasch, 2020;

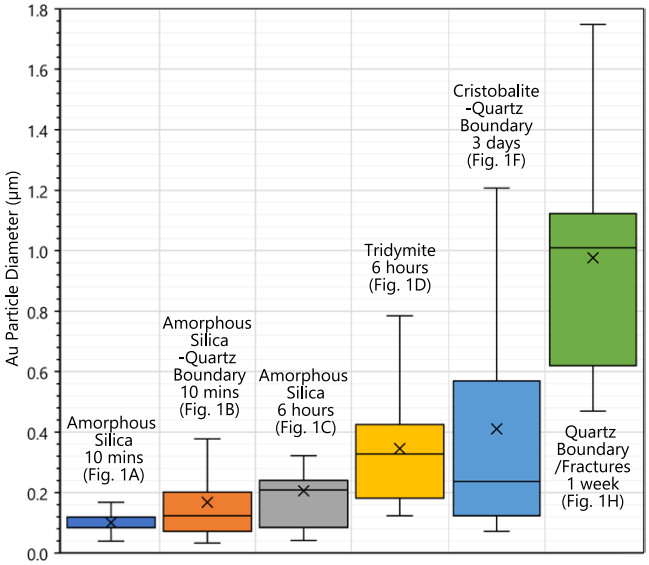

Figure 2. Particle diameter distribution for Au in select backscatter-electron (BSE) images. Mean particle size is represented by "x." Data are summarized in Table S3 (see text footnote 1).

Faber et al., 2014), but OGDs form deeper and at higher temperatures, conditions where precipitation of $aSiO_2$ is unlikely to be widespread (Williams and Fagereng, 2022). However, OGDs represent exceptional hydrothermal systems, characterized by high fluid fluxes, high fluid:rock ratios, and repeated and long-lived hydrothermal activity (Mernagh et al., 2004). These features represent favorable conditions for $aSiO_2$ precipitation and thus may explain the rarity of OGDs. Our experiments showed that preservation of $aSiO_2$ is unlikely at these conditions, as $aSiO_2$ reacts to form stable quartz within days at 400 °C (Fig. 3A). Such rapid recrystallization is consistent with previous experimental work (Bettermann and Liebau, 1975; Williams et al., 2015). Hence, preservation of $aSiO_2$ in orogenic systems is unlikely. Nonetheless, Petrella et al. (2020, 2022) found $aSiO_2$ inclusions associated with AuNPs within coarse Au grains in multiple OGDs, showing nanotextures (Fig. 3B) consistent with those from our experiments at 10 min at 400 °C (Figs. 1A and 1B). The characteristic microtextures associated with recrystallization of tridymite from the rims of $aSiO_2$ spheres seen in our experiments (Fig. 1C) are preserved in veins at the Voltri OGD in Italy (Fig. 3C; Herrington and Wilkinson, 1993). Additionally, the quartz-Au microtextures resulting from complete recrystallization of $aSiO_2$ to quartz after 1 wk at 400 °C (coarse native Au along quartz grain boundaries and within fractures in quartz; Fig. 1H) are widespread in high-grade orogenic Au ores worldwide (Fig. 3D; Herrington and Wilkinson, 1993).

Crustal fluids are likely to be saturated with respect to quartz rather than $aSiO_2$ at 300–400 °C. At conditions relevant for OGD formation, a fluid saturated with $aSiO_2$ will have about twice the SiO_2 content of a fluid saturated with respect to quartz (Karásek et al., 2013). Our experiments had SiO_2 concentrations ~13 times that of quartz saturation, but the silica textures observed match experiments conducted with SiO_2 concentrations of only ~3 times that of quartz saturation (Okamoto et al., 2010), which suggests that the formation behavior of $aSiO_2$ is consistent at variable fluid supersaturation.

Amorphous silica precipitation requires a shift from quartz to $aSiO_2$ saturation fast enough to preclude equilibrium quartz precipitation. In natural orogenic systems, conditions responsible for this have been suggested to be fluids undergoing rapid, transient depressurization from

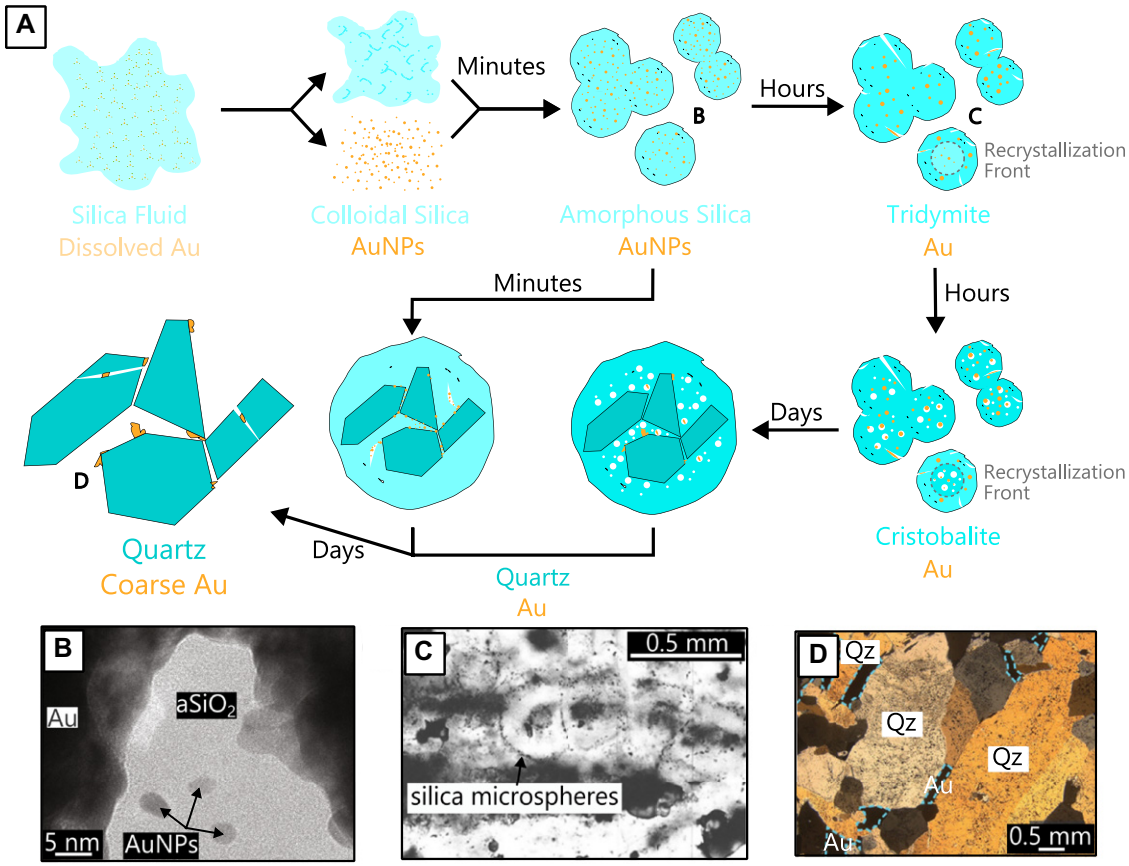

Figure 3. (A) Schematic showing steps involved in forming Au-quartz from Au–colloidal silica gel observed here. (B) Au nanoparticles (AuNPs) in amorphous silica ($aSiO_2$) from within Au grain from Discovery deposit, Canada (Petrella et al., 2022). (C) Microspheres from within vein from Voltri deposits, Italy (Herrington and Wilkinson, 1993). (D) Coarse Au on grain boundaries of quartz (Qz) from within veins from Fosterville deposit, Australia.

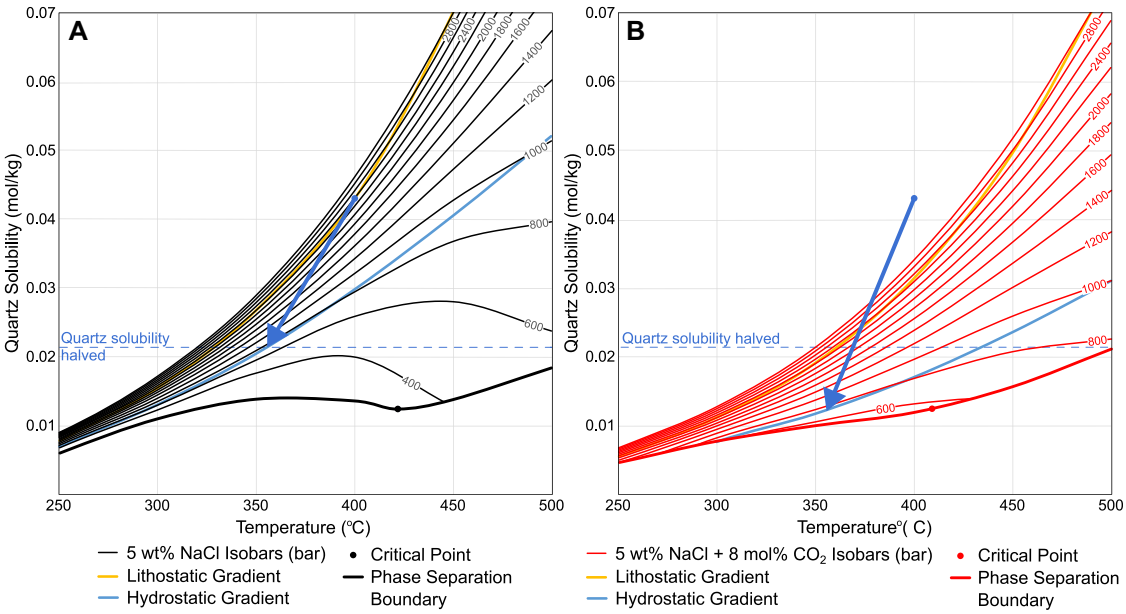

Figure 4. Quartz solubility halving with (A) lithostatic-hydrostatic pressure decrease and (B) increasing CO_2 content, based on Akinfiev and Diamond (2009).

lithostatic to hydrostatic pressures during "fault-valving" (2400 bar and 400 °C to 715 bar and 358 °C in 5 wt% NaCl; Fig. 4A; Herrington and Wilkinson, 1993; Okamoto et al., 2010; Williams and Fagereng, 2022). In the fault-valve model, supralithostatic fluid pressures may develop when upwardly migrating deep fluids are trapped by an impermeable barrier (Cox et al., 1995). The resulting overpressure facilitates fault slip and fracture formation, allowing upward fluid migration and opening of extensional fractures, which leads to drops in fluid pressure and temperature (Cox, 2016; Sibson et al., 1988). Note that there are several limitations regarding the kinetics of depressurization associated with fault-valving as a mineralization mechanism in orogenic systems (Williams and Fagereng, 2022). Pressure drops well below the lithostatic load should also result in fracture collapse, leaving little pore space available for mineralization (Fisher et al., 2019). Finally, the mass balance of silica in pore fluids during dilation and depressurization of isolated extensional fractures suggests this process can only result in mineralization of ~0.005% of a void with $aSiO_2$ (Williams, 2019), which would require multiple events to generate reasonable $aSiO_2$ mineralization.

Temperature decreases can also lead to fluid oversaturation with respect to $aSiO_2$. They may occur during rapid upward fluid migration, as OGDs can record fluid temperature gradients of up to 100 °C/km (Mernagh et al., 2004), or adiabatic cooling (~up to 164 °C in the example shown in Fig. 4A). Note that maximum precipitation rates are achieved at drops of ~50 °C below the $aSiO_2$ saturation point, due to decreasing reaction kinetics at larger temperature drops (Rimstidt and Barnes, 1980).

Addition of CO_2 can also promote silica supersaturation in pore fluids (e.g., addition of 8 mol% CO_2 to previous example; Fig. 4B). CO_2 can be driven from the wall rock into fractures by oxidation of reduced carbon, e.g., graphite in host slates/shales (Petrella et al., 2021), and during the reversal of hydraulic head that occurs pre- to synrupture (Cox et al., 1995). This may explain why high-grade Au-quartz veins in OGDs can be spatially associated with carbonaceous rocks and graphite (Petrella et al., 2021). The absence of sulfur in our experiments restricts our description of Au deposition alongside $aSiO_2$ as sulfur species represent important Au complexing ligands in hydrothermal fluids (Williams-Jones et al., 2009). However, Au is expected to precipitate alongside $aSiO_2$, as lower fluid density and CO_2 addition cause an exponential decrease in the solubility of $Au(HS)_{(aq)}$ due to disruption in the hydration sphere (Liu et al., 2008; Mei et al., 2017).

In summary, the evidence for $aSiO_2$ in OGDs, in conjunction with the new experimental work presented here, highlights the possibility that $aSiO_2$ does precipitate in orogenic systems. The dynamic conditions prevailing during this process are likely to provide transient microenvironments favorable to the deposition and enrichment of both $aSiO_2$ and Au. More work is required, however, to constrain the exact mechanisms that give rise to such high silica supersaturations in pore fluid, and the processes by which these factors control the distribution of high-grade ores in some OGD systems.

Au Enrichment and Remobilization

Our experiments provide insights into the potential key roles played by colloidal silica and AuNPs in the initial stage of high-grade ore formation. The precipitation and entrapment of AuNPs in $aSiO_2$ during deposition of colloidal silica in our experiments (Fig. 1A; Table S1) represent important Au entrapment mechanisms that may be applicable to OGD formation. Our results replicate the textures found in natural Au-rich quartz veins and support the previous hypotheses put forth by Herrington and Wilkinson (1993). Without the changes in conditions required for $aSiO_2$ precipitation, Au may not be efficiently trapped and enriched in quartz veins, resulting in dispersed Au and barren quartz veins. Additionally, rapid $aSiO_2$ precipitation should also suddenly decrease the permeability of Au-fluid pathways, further entrapping Au, similar to observations from fractured granite and flash vaporization experiments (Amagai et al., 2019; Watanabe et al., 2021).

Remobilization of Au is an important process in allowing significant Au accumulation locally into high-grade zones of OGDs. Remobilization of AuNPs within silica in orogenic gold ores has been theorized previously (Herrington and Wilkinson, 1993; Petrella et al., 2020), but our experiments represent the first evidence of this secondary Au remobilization mechanism. Ostwald ripening by solid-state diffusion of Au resulted in the coarsening of AuNPs in an arsenian pyrite host at ~500 °C (Reich et al., 2006). A similar coarsening affected AuNPs in $aSiO_2$ in our experiments, during $aSiO_2$-tridymite recrystallization, during recrystallization of tridymite to cristobalite, and along quartz grain boundaries (Fig. 2). Whereas the annealing experiments conducted by Reich et al. (2006) were conducted under dry conditions, our experiments were fluid-rich, and recrystallization of $aSiO_2$ will also generate water at the reaction interface. Hence, Au mobility in our experiments was probably fluid-enhanced and was likely focused along grain boundaries, resulting in the observed concentration of AuNPs at recrystallization fronts (Figs. 1B, 1C, 1E, 1F, and 1H). The best example of this occurred during the growth of quartz, as Au was not incorporated into quartz crystals and moved toward grain boundaries

(Figs. 1B, 1F, and 1H). The combined power of fluid-enhanced Ostwald ripening and rejection from quartz allowed Au concentration during initial OGD formation and the transition from AuNPs within metastable silica phases to coarse Au along quartz grain boundaries in a matter of days at 400 °C (Fig. 3), which is practically instantaneous on geological time scales.

Implications

Quartz recrystallization from $aSiO_2$ and the grain boundary migration observed in our experiments may help to explain the growth and physical properties of veins. Faults are expected to have a brief period (hours to weeks) of low yield strength during the time from $aSiO_2$ precipitation to quartz recrystallization (Di Toro et al., 2004), which may facilitate repeated local failure during earthquake aftershock periods or swarms. With each failure, fresh circulating fluids may precipitate Au, leading to further enrichment in quartz veins.

Although these experiments focused on Au enrichment in quartz veins, they are applicable to metal mobility in quartz-hosted hydrothermal deposits throughout the seismogenic zone of the crust (3–20 km depth; Masuda et al., 2019). These findings demonstrate the importance of considering the potential for $aSiO_2$ precipitation and subsequent quartz recrystallization to alter the behavior of other metal deposition processes in OGDs, and more broadly in other hydrothermal deposits throughout the crust.

ACKNOWLEDGMENTS

Research funding was provided by the Australian Research Council (LP200200897). The authors acknowledge use of the Monash Centre for Electron Microscopy and X-ray Platform and valuable feedback from R. Williams, R. Herrington, and E. Hastie.

REFERENCES CITED

Akinfiev, N.N., and Diamond, L.W., 2009, A simple predictive model of quartz solubility in water-salt-CO_2 systems at temperatures up to 1000°C and pressures up to 1000 MPa: Geochimica et Cosmochimica Acta, v. 73, no. 6, p. 1597–1608, https://doi.org/10.1016/j.gca.2008.12.011.

Amagai, T., Okamoto, A., Niibe, T., Hirano, N., Motomiya, K., and Tsuchiya, N., 2019, Silica nanoparticles produced by explosive flash vaporization during earthquakes: Scientific Reports, v. 9, no. 1, 9738, https://doi.org/10.1038/s41598-019-46320-7.

Bettermann, P., and Liebau, F., 1975, The transformation of amorphous silica to crystalline silica under hydrothermal conditions: Contributions to Mineralogy and Petrology, v. 53, no. 1, p. 25–36, https://doi.org/10.1007/BF00402452.

Borhara, K., and Onasch, C.M., 2020, Evidence for silica gel and its role in faulting in the Tuscarora Sandstone: Journal of Structural Geology, v. 139, https://doi.org/10.1016/j.jsg.2020.104140.

Cox, S.F., 2016, Injection-driven swarm seismicity and permeability enhancement: Implications for the dynamics of hydrothermal ore systems in high fluid-flux, overpressured faulting regimes—An invited paper: Economic Geology, v. 111, no. 3, p. 559–587, https://doi.org/10.2113/econgeo.111.3.559.

Cox, S.F., Sun, S.S., Etheridge, M.A., Wall, V.J., and Potter, T.F., 1995, Structural and geochemical controls on the development of turbidite-hosted gold quartz vein deposits, Wattle Gully Mine, central Victoria, Australia: Economic Geology, v. 90, no. 6, p. 1722–1746, https://doi.org/10.2113/gsecongeo.90.6.1722.

Di Toro, G., Goldsby, D.L., and Tullis, T.E., 2004, Friction falls towards zero in quartz rock as slip velocity approaches seismic rates: Nature, v. 427, no. 6973, p. 436–439, https://doi.org/10.1038/nature02249.

Faber, C., Rowe, C.D., Miller, J.A., Fagereng, Å., and Neethling, J.H., 2014, Silica gel in a fault slip surface: Field evidence for palaeo-earthquakes?: Journal of Structural Geology, v. 69, p. 108–121, https://doi.org/10.1016/j.jsg.2014.09.021.

Fisher, D.M., Smye, A.J., Marone, C., van Keken, P.E., and Yamaguchi, A., 2019, Kinetic models for healing of the subduction interface based on observations of ancient accretionary complexes: Geochemistry, Geophysics, Geosystems, v. 20, no. 7, p. 3431–3449, https://doi.org/10.1029/2019GC008256.

Frimmel, H.E., 2008, Earth's continental crustal gold endowment: Earth and Planetary Science Letters, v. 267, no. 1–2, p. 45–55, https://doi.org/10.1016/j.epsl.2007.11.022.

Hastie, E.C.G., Schindler, M., Kontak, D.J., and Lafrance, B., 2021, Transport and coarsening of gold nanoparticles in an orogenic deposit by dissolution-reprecipitation and Ostwald ripening: Communications Earth & Environment, v. 2, no. 1, p. 57, https://doi.org/10.1038/s43247-021-00126-6.

Herrington, R.J., and Wilkinson, J.J., 1993, Colloidal gold and silica in mesothermal vein systems: Geology, v. 21, no. 6, p. 539–542, https://doi.org/10.1130/0091-7613(1993)021<0539:CGASIM>2.3.CO;2.

Karásek, P., Šťavíková, L., Planeta, J., Hohnová, B., and Roth, M., 2013, Solubility of fused silica in sub- and supercritical water: Estimation from a thermodynamic model: The Journal of Supercritical Fluids, v. 83, p. 72–77, https://doi.org/10.1016/j.supflu.2013.08.012.

Liu, W., Brugger, J., Etschmann, B., Testemale, D., and Hazemann, J.-L., 2008, The solubility of nantokite (CuCl(s)) and Cu speciation in low-density fluids near the critical isochore: An in-situ XAS study: Geochimica et Cosmochimica Acta, v. 72, no. 16, p. 4094–4106, https://doi.org/10.1016/j.gca.2008.05.056.

Liu, W., Chen, M., Yang, Y., Mei, Y., Etschmann, B., Brugger, J., and Johannessen, B., 2019, Colloidal gold in sulphur and citrate-bearing hydrothermal fluids: An experimental study: Ore Geology Reviews, v. 114, https://doi.org/10.1016/j.oregeorev.2019.103142.

Masuda, K., Arai, T., and Takahashi, M., 2019, Effects of frictional properties of quartz and feldspar in the crust on the depth extent of the seismogenic zone: Progress in Earth and Planetary Science, v. 6, no. 1, p. 50, https://doi.org/10.1186/s40645-019-0299-5.

Mei, Y., Liu, W., Brugger, J., Migdisov, A.A., and Williams-Jones, A.E., 2017, Hydration is the key for gold transport in CO_2-HCl-H_2O vapor: ACS Earth & Space Chemistry, v. 1, no. 7, p. 368–375, https://doi.org/10.1021/acsearthspacechem.7b00020.

Mernagh, T.P., Heinrich, C.A., and Mikucki, E.J., 2004, Temperature gradients recorded by fluid inclusions and hydrothermal alteration at the Mount Charlotte gold deposit, Kalgoorlie, Australia: Canadian Mineralogist, v. 42, no. 5, p. 1383–1404, https://doi.org/10.2113/gscanmin.42.5.1383.

Okamoto, A., Saishu, H., Hirano, N., and Tsuchiya, N., 2010, Mineralogical and textural variation of silica minerals in hydrothermal flow-through experiments: Implications for quartz vein formation: Geochimica et Cosmochimica Acta, v. 74, no. 13, p. 3692–3706, https://doi.org/10.1016/j.gca.2010.03.031.

Petrella, L., Thébaud, N., Fougerouse, D., Evans, K., Quadir, Z., and Laflamme, C., 2020, Colloidal gold transport: A key to high-grade gold mineralization?: Mineralium Deposita, v. 55, no. 7, p. 1247–1254, https://doi.org/10.1007/s00126-020-00965-x.

Petrella, L., Thébaud, N., Evans, K., LaFlamme, C., and Occhipinti, S., 2021, The role of competitive fluid-rock interaction processes in the formation of high-grade gold deposits: Geochimica et Cosmochimica Acta, v. 313, p. 38–54, https://doi.org/10.1016/j.gca.2021.08.024.

Petrella, L., Thébaud, N., Fougerouse, D., Tattitch, B., Martin, L., Turner, S., Suvorova, A., and Gain, S., 2022, Nanoparticle suspensions from carbon-rich fluid make high-grade gold deposits: Nature Communications, v. 13, no. 1, p. 3795, https://doi.org/10.1038/s41467-022-31447-5.

Pokrovski, G.S., Akinfiev, N.N., Borisova, A.Y., Zotov, A.V., and Kouzmanov, K., 2014, Gold speciation and transport in geological fluids: Insights from experiments and physical-chemical modelling, *in* Garofalo, P.S., and Ridley, J.R., eds., Gold-Transporting Hydrothermal Fluids in the Earth's Crust: Geological Society, London, Special Publication 402, p. 9–70, https://doi.org/10.1144/SP402.4.

Rauchenstein-Martinek, K., Wagner, T., Wälle, M., and Heinrich, C.A., 2014, Gold concentrations in metamorphic fluids: A LA-ICPMS study of fluid inclusions from the Alpine orogenic belt: Chemical Geology, v. 385, p. 70–83, https://doi.org/10.1016/j.chemgeo.2014.07.018.

Reich, M., Utsunomiya, S., Kesler, S.E., Wang, L., Ewing, R.C., and Becker, U., 2006, Thermal behavior of metal nanoparticles in geologic materials: Geology, v. 34, no. 12, p. 1033–1036, https://doi.org/10.1130/G22829A.1.

Rimstidt, J.D., and Barnes, H.L., 1980, The kinetics of silica-water reactions: Geochimica et Cosmochimica Acta, v. 44, no. 11, p. 1683–1699, https://doi.org/10.1016/0016-7037(80)90220-3.

Sibson, R.H., Robert, F., and Poulsen, K.H., 1988, High-angle reverse faults, fluid-pressure cycling, and mesothermal gold-quartz deposits: Geology, v. 16, no. 6, p. 551–555, https://doi.org/10.1130/0091-7613(1988)016<0551:HARFFP>2.3.CO;2.

Tooth, B., Brugger, J., Ciobanu, C., and Liu, W., 2008, Modeling of gold scavenging by bismuth melts coexisting with hydrothermal fluids: Geology, v. 36, no. 10, p. 815–818, https://doi.org/10.1130/G25093A.1.

Watanabe, N., Abe, H., Okamoto, A., Nakamura, K., and Komai, T., 2021, Formation of amorphous silica nanoparticles and its impact on permeability of fractured granite in superhot geothermal environments: Scientific Reports, v. 11, no. 1, p. 5340, https://doi.org/10.1038/s41598-021-84744-2.

Williams, R.T., 2019, Coseismic boiling cannot seal faults: Implications for the seismic cycle: Geology, v. 47, no. 5, p. 461–464, https://doi.org/10.1130/G45936.1.

Williams, R.T., and Fagereng, Å., 2022, The role of quartz cementation in the seismic cycle: A critical review: Reviews of Geophysics, v. 60, no. 1, https://doi.org/10.1029/2021RG000768.

Williams, R.T., Farver, J.R., Onasch, C.M., and Winslow, D.F., 2015, An experimental investigation of the role of microfracture surfaces in controlling quartz precipitation rate: Applications to fault zone diagenesis: Journal of Structural Geology, v. 74, p. 24–30, https://doi.org/10.1016/j.jsg.2015.02.011.

Williams-Jones, A.E., Bowell, R.J., and Migdisov, A.A., 2009, Gold in solution: Elements, v. 5, no. 5, p. 281–287, https://doi.org/10.2113/gselements.5.5.281.

Printed in the USA